Available online at www.sciencedirect.com

SciVerse ScienceDirect

Physics Procedia 39 (2012) 903 – 912

Physics Procedia

LANE 2012

Modeling of crystal orientations in laser powder deposition of single crystal material

Huan Qi*, Zhaoyang Liu

University of Michigan, Shanghai Jiaotong University Joint Institute, 800 Dongchuan Road, Shanghai, 200240, P.R. China

Abstract

This paper presents a numerical model which simulates the dynamic molten pool formation and the crystal orientations of solidified SX alloy in a multi-layer laser powder deposition process. Based on the mathematical model of coaxial laser direct deposition, the effect of parameters (laser power, scanning speed, powder feed rate) on the tendency to form [001] direction expitaxial grains during solidification was evaluated. In the transient three-dimensional model, physical phenomena including heat transfer, melting, grain formation during solidification, mass addition, and fluid flow in the melt pool, were modeled in a self-consistent manner. The temperature fields, fluid flow velocity, clad geometry (width, height and melt pool depth) and grain formation in melting pool of single layer are predicted.

Keywords: Laser powder deposition; single crystal; grain orientation; modeling

1. Introduction

Repair of turbine blades made of single crystal (SX) or directionally solidified (DS) alloy has drawn a great deal of attentions due to the great value (up to 80%) it saves compared to the costly new blade replacement. Laser direct metal deposition has shown to be an effective technology to restore the worn blade squealer tips in a net shape way and be able to produce sound material properties that meet repair requirements [1,2]. However, this technology has only been used to deposit polycrystalline alloys in turbine blade repair applications. The polycrystalline material once deposited on single crystal turbine blade causes degraded material mechanical properties and reduced creep-fatigue life of parts due to the appearance of grain boundaries. The ideal SX blade repair technology ought to produce a similar

* Corresponding author. Tel.: +86-21-34206524 ; fax: +86-21-34206525 .
E-mail address: huan.qi@sjtu.edu.cn .

 doi:10.1016/j.phpro.2012.10.115

crystalline structure to the base material, which requires the SX or DS crystal orientation of the base material being retained and continuously growing during the solidification of laser metal deposition. Formation of disorientated grains or stray grains should be avoided which are due to the undercooling solidification nucleus formed in the molten pool. Stray grains in SX, once formed, produce grain boundaries with low melting temperature which weakens material strength and causes strain age crack in repaired material.

Formation of epitaxial grains in SX deposition is affected by the solidification variables of a molten pool. Gaumann et al reported [3-4] that solidification velocity and temperature gradient at the solidification front are the two fundamental variables determining the grain solidification direction. These solidification variables are complex functions of laser deposition parameters, material properties, and positions in a three-dimensional molten pool. They have identified the necessary CET (Columnar to Equiaxed Transition) condition as a result of appropriate laser deposition parameters to produce a SX deposition. Liu and Dupont [5-6] studied the effects of molten pool geometry on crystalline growth direction in laser remelted SX material. They proposed a predefined 3-D molten pool geometry model and verified the predicted grain orientations with the experimental results. Vitek et al [7-8] find that stray grain formation is very sensitive to crystallographic orientation of growing dendrites as well as processing conditions. With low power and welding speed, no stray grain was found in the weld. Anderson et al [9] studied the laser SX remelting parameters and their effect on stray grain formation, combining experimental results and Gaumann's CET model. Most of these models are based on laser remelting of SX material where no additive material (powder) has been introduced into the melt pool. The formation of a hump molten pool and its free surface evolution play a significant role in affecting the solidification variables and the resulted crystalline orientations. This becomes a more substantial factor when multi-layer deposition is desired to continuously grow the SX or DS structure in blade tip repair.

Many numerical models have been reported with the capability of revealing the laser powder deposition process dependences on related parameters. Most of the models can predict molten pool temperature, cooling rate, deposit feature sizes, and depth of dilution [10-13]. Wen et al [14] use an improved level-set method, which takes the conservative form while being implicitly solved with other governing equations. Simulated track heights, widths, molten pool depths, and clad profiles agree well with experiment ones. He et al [15] developed a comprehensive three-dimensional numerical model for double-track laser cladding process of H13 steel. However, few can simulate the dynamic molten pool morphology and the resulted crystalline growth orientation in a multi-layer deposition configuration. This paper presents a complex numerical model which simulates the dynamic molten pool formation and the crystal orientations of solidified SX alloy in a multi-layer laser powder deposition process.

2. Modeling Method

A schematic of the laser powder deposition with coaxial powder feeding is shown in fig.1. In this physical model, substrate is stationary in a three-dimensional Cartesian coordinate with a SX orientation of [001] direction normal to the surface. A focused laser beam is striking on the substrate and scanning in the X direction at a constant speed. The laser beam heats a small area of the substrate and produces a melt pool. Metal powder is delivered through gas flow coaxially with the laser beam and falling into the melt pool. A deposited track is formed as a result of continuous melting of captured powder and solidification of molten pool with the moving of laser beam. The melts solidifies very quickly due to the high associated cooling rate (104 K/s). The laser beam, which is assumed as Gaussian distribution and with a half divergence angle of 2.7º, is focused to a spot size of 0.6 mm at 9 mm below the nozzle tip. The liquid motion in the melt pool is assumed to be incompressible Newtonian fluid. Powders get melted as soon as

falling into the melt pool. The fluid flow is considered to be laminar, and is driven by the buoyancy force, temperature gradient and surface tension on melt pool surface (Manangoni force), powder gravity and inertia force, and shield gas impinging force. The thermal-physical properties and the absorption coefficient of material are assumed to be temperature dependent. The thermal-physical properties of powders are considered the same to those of the substrate.

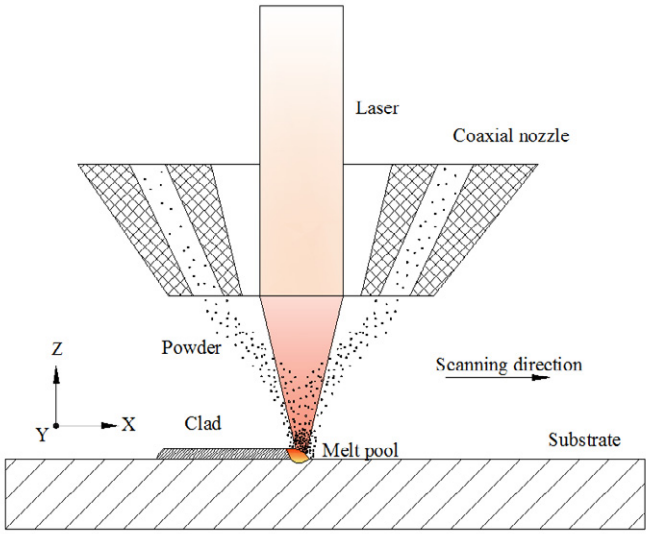

Fig.1. A schematic of the coaxial powder injection laser cladding process

Based on the mathematical model of coaxial laser powder deposition, the effect of parameters (laser power, scanning speed, powder feed rate) on the tendency to form [001] epitaxial grains during solidification was evaluated. In the transient three-dimensional model, physical phenomena including heat transfer, melting, grain formation during solidification, mass addition, and fluid flow in the melt pool, were modeled in a self-consistent manner. Interactions between the laser beam and coaxial powder flow, including the attenuation of beam intensity and temperature rise of powder particles before reaching the melt poor were modeled with a simple heat balance equation. An improved level-set function, which calculates the moving interface accurately under the influence of surface tension, fluid flow velocity and Manangoni forces on redistribution of added mass, is employed to track the dynamic evolution of molten pool surface during laser deposition process. A moving structure grid technology is used in calculating the grain formation in the melt pool. Details of this model on heat transfer, fluid flow, melting and solidification are based on the authors' previous work [11].

2.1. Melt pool surface tracking

Level-set method was used to accurately track the evolution of the melt pool surface. The general form of the level-set equation is given below,

$$\frac{\partial \phi}{\partial t} + F \nabla \phi = 0 \tag{1}$$

where ϕ is the level set function representing the actual distance from the zero level set surface, F is the speed function normal to the free surface. In laser deposition, the speed function consists of two parts: one is local melt pool speed function and the other is powder mass addition, as shown in Eq (2).

$$F = F_p + \vec{n} \cdot \vec{V}(x, y, z, t) \tag{2}$$

where F_p is the free surface growth velocity due to the powder addition, $\vec{n}$ is the normal of the interface, V is the local redistribution velocity on the liquid free surface, and is determined by the Navier-Stokes equations. The free surface growth velocity due to powder mass addition is given by

$$F_p = \frac{V_{powder}}{\frac{e-1}{2e^2}\pi R_p^2} \exp\left(\frac{-2r^2}{R_p^2}\right) \tag{4}$$

in which V_{powder} is the powder volume flow rate captured by the melt pool, r is the radial distance from the powder stream center, R_p is the radius of the powder stream.

2.2. Grain growth model

The grain crystallographic direction of the deposit is directly influenced by the solidification conditions prevailing at the transformation front, such as temperature gradient G and solidification velocity V_S. A columnar and equiaxed dendrite transformation model [16] is used in the physical model. The following equation is used to determine the grain growth directions during the melt pool solidification,

$$\frac{G^n}{V_{iso}}\left(\cos\psi\right)^{n+1} > K_{CET}, \text{ where } K_{CET} = a \times \left[\left(\frac{-4\pi N_0}{3\ln(1-\varphi_c)}\right)^{\frac{1}{3}} \frac{\Delta T_0}{n+1}\right]^n \tag{5}$$

where the constant K_{CET} is a function of the alloy parameters and of the transition criterion φ_c is the critical volume fraction of equiaxed grains, G is the temperature gradient, N_0 is the number of nucleation sites, a and n are alloy parameters, ΔT_0 is undercooling temperature, and Ψ is crystal anisotropy.

2.3. Solution technique

In order to reduce the calculating time, a small domain containing the melt pool is used to calculate the grain growth direction in melt pool accurately. The small domain moves with the melt pool and is updated at every time step, which can improve the calculation accuracy of grain growth model without

increasing the number of actual grids. The size of small domain grid is half of the original size, and 1/8 in volume of the original grid. The temperature filed, fluid flow and level-set function were calculated in whole domain. Then the data of temperature filed and surface motion of the melt pool was transferred into small domain by linear difference algorithm. The temperature of the sub-grid in small domain can be calculated as

$$T_{sub-grid} = \frac{\sum_{i}^{n} L_i^{-1} T_i}{\sum_{i}^{n} L_i^{-1}}, \quad (6)$$

where Li is the distance between the sub and original grids, Ti is the temperature of the ith grid in the whole domain, n is the grid number around the ith grid.

In this numerical model, control-volume based finite differential method is used in discretization of the governing equations. In order to accurately calculate the temperature filed and free surface motion of the melt pool, the grid size at the laser irradiated area must be adequately small. The minimum grid size is 20um. It is assumed that the domain is symmetrical in the Y direction, therefore only half of the domain is considered. A computational domain in the size of 13x5x10 mm in X Y, and Z, is meshed with a nonuniform grid system of 93x37x53. Flow chart of the numerical solution procedure in each time step is shown in fig 2.

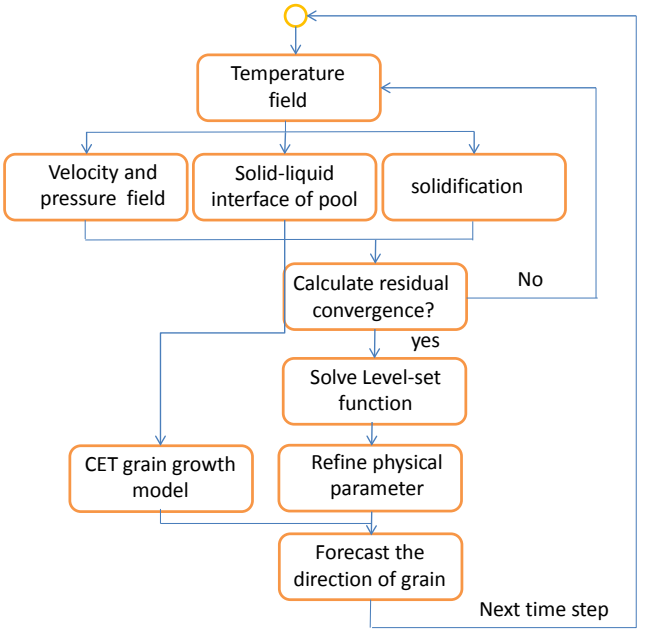

Fig. 2. Flowchart of the calculation procedure in each time step

3. Experimental Procedure

The powder of single crystal superalloy Rene N5 was used in this experiment. A typical commercial DS nickel-base superalloy, GTD 111 alloy, was used as the substrate alloy. A 12 mm diameter rod with [001] crystallographic direction aligned in the axial direction was cut into 4 mm thick wafers. The laser deposition was performed on the (001) substrate surface of the wafers. The substrate surface was ground with 300-grit SiC paper and cleaned by acetone and alcohol before laser deposition. Single layer deposits were produced with various parameters in the study.

After completing the first layer, the layer thickness was measured. The laser nozzle was incremented upward in the height direction in an amount of the layer thickness. A new layer was subsequently deposited onto the previous layer. The laser deposition processing was protected by shielding argon gas provided through the coaxial nozzle. Samples were mounted, polished and etched using standard metallographic techniques for nickel based superalloys. Light optical microscopy was used for microstructure analysis in the study.

4. Results and Discussion

The temperature field, fluid flow velocity field, geometry of molten pool and grain formation in one or two layer deposition were obtained through the above described model. Fig. 3a shows the temperature field and velocity fields of single track laser powder deposition with a set of typical processing parameters, i.e. laser power 200w, and beam spot size 0.6mm, scanning speed 5mm /s, and powder flow rate 6g/min. The maximum temperature in the melt pool is 2078.3℃. As can be seen in fig. 3b-c, the shape of the melt pool and the fluid flow inside vary significantly with a scanning speed changed from 10mm/s to7.5mm/s.

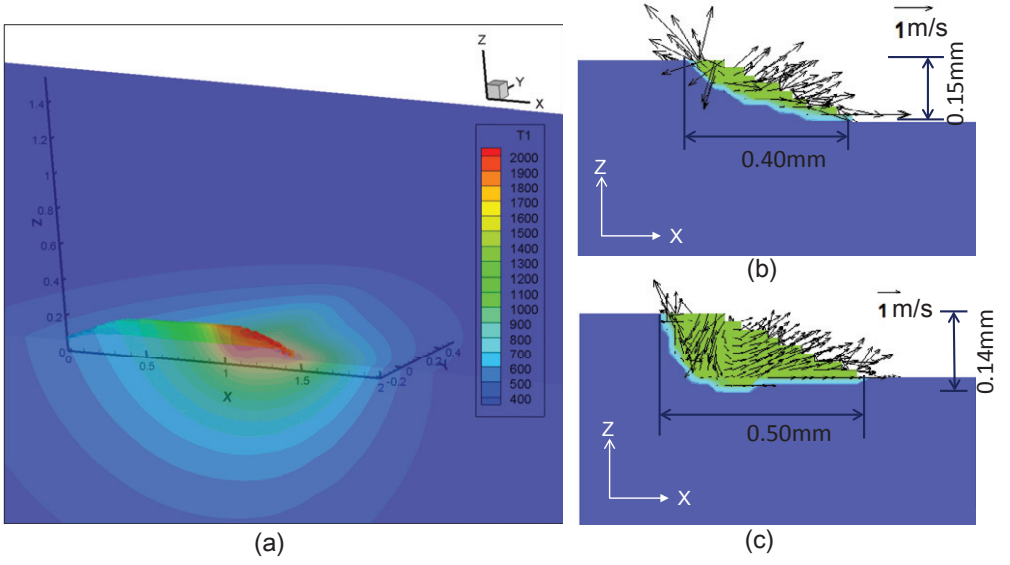

Fig. 3. (a) temperature field of single track laser powder deposition with laser power = 200w, beam spot size = 0.6mm, scanning speed = 5mm/s, and powder flow rate = 6g/min; (b) and (c) velocity fields in melt pool with scanning speed = 10mm/s and 7.5mm/s respectively, velocity vectors pointing outwards at the melt pool free surface indicate the interface growth velocity due to the powder addition in the melt pool

Comparison of the height, width and the melting depth of the single track deposition between the simulation and experimental results are shown in Table 1. It can be seen that the deposit height, width, and substrate melting depth agree reasonably well between the experimental and simulation results. Distributions of grain orientations in the cross-section of single track laser deposition between simulation and experimental results are compared graphically in fig 4. The [001] direction grain grows epitaxially from liquid/solid (L/S) interface and up to about half height of the deposit track. The simulation result shows a small portion of [010] direction grain forms at the jointing edges of the deposit and substrate interface, which matches the experiment results. It indicates the competitive growth between different crystallographic directions as a result of the dynamic L/S interface. The grain growth condition varies at different altitude of the melt pool, depending on the variation of temperature gradient G and solidification velocity VS on the L/S interface, as well as the inclining angle between normal direction of L/S interface and laser scanning direction. At certain height of the deposit layer, the [001] direction grains transform into equiaxial grains.

Table 1. Comparison of the characteristic dimensions of single layer deposit between simulation and experimental results

	Deposit Track Height (mm)	Deposit Track Width (mm)	Substrate melting depth (mm)
Experimental	0.268	0.754	0.125
Simulation	0.225	0.658	0.113
Error	16.0%	12.7%	9.6%

Note: Deposition parameters: Laser power 200W, beam spot size 0.6 mm, scanning speed 5 mm/s, and powder flow rate 6 g/min

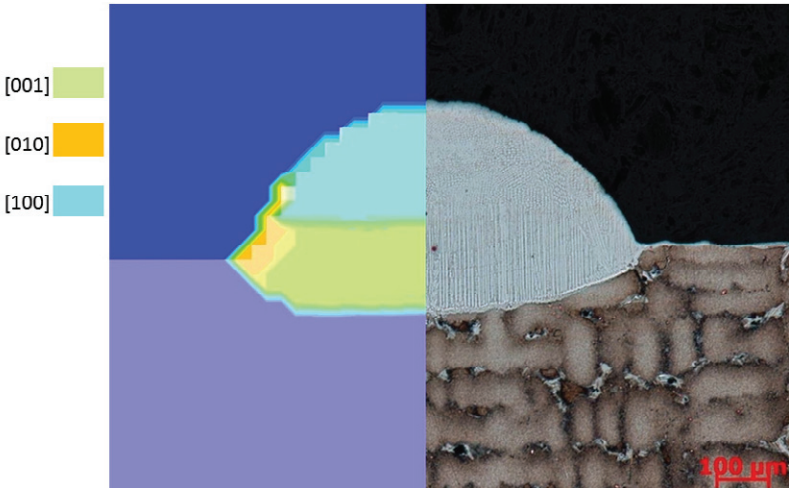

Fig. 4. Comparison of the cross-section geometry and grain orientations of single track deposit between simulated and experiment results, processing parameters: Laser power 200W, beam spot size 0.6 mm, scanning speed 5 mm/s, and powder flow rate 6 g/min

Fig. 5a shows the effect of laser power (a 10.6 μm wavelength CO2 laser is used in this calculation) on the depth of the [001] solidification direction grains formed in a single track deposition. Percentage of [001] direction grain in the cross-section of a single track laser deposition with different levels of linear energy (J/mm) are obtained through the modeling method as shown in fig. 5b. It can be seen that

increasing laser power or linear energy makes the depth of [001] direction grain decrease in the deposition track, which is a result of significant change of the melt pool shape as shown in fig. 3. Deposition with relatively lower laser power leads to faster cooling rate and therefore shallower melt pool. The solid/liquid interface is formed with a small inclining angle relative to the laser scanning direction, which makes the maximum temperature gradient direction (normal to the L/S interface) close to the SX solidification preference direction in <001>. This leads to higher crystalline growth in the vertical direction in the deposition track. The simulation results are close to the experimental results at low linear energy, but variant at high linear energy. More linear energy enlarges melt pool, the L/S interface in clad layer becomes more vertical, which leads columnar-euquaixial transition to happens at the position near to the bottom of melt pool.

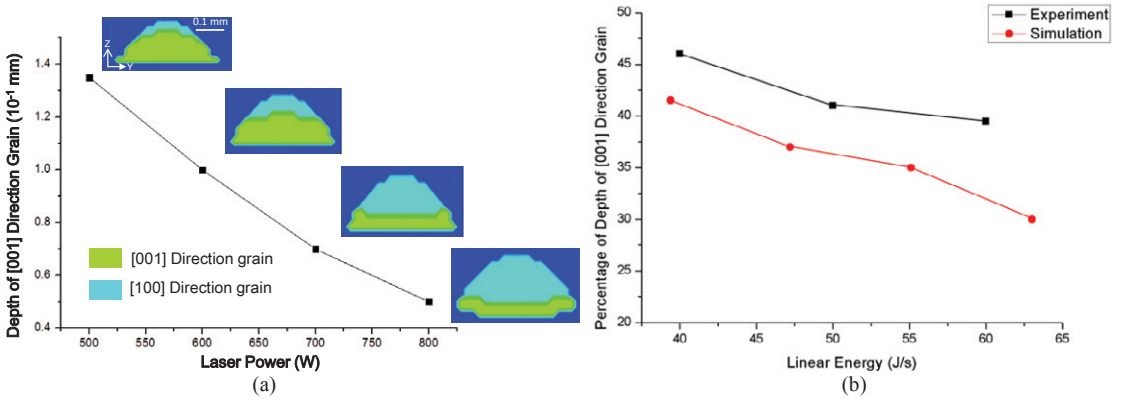

Fig. 5. (a) effect of laser power (a 10.6 μm wavelength CO_2 laser is used in this calculation) on the depth of [001] solidification direction grain. Colored pictures shown the distribution of grain growth direction in the cross-section of a SX laser deposition layer with different levels of laser power, while beam spot size 0.5 mm, scanning speed 12.7 mm/s, and powder flow rate 7g/min. (b) comparison of the percentage of the depth of [001] direction grain in the cross-section of a SX laser deposition layer between simulated and experiment results. Laser power 200 W (a 1070 nm wavelength fiber laser is used in this), beam spot 0.6 mm, scanning speed 5 mm/s, and powder flow rate 6 g/min

Fig. 6 shows the cross-section geometry and grain orientation distributions of double layer deposition from simulation and experimental results respectively. The same processing parameters of the single track deposition were used. Compared to the single track deposition, heat transfer by conduction is reduced when the second layer is being deposited, since the effective heat conduction area below the melt pool is decreased. This leads to higher temperature and larger size of the melt pool formed in the second layer. In the simulation, after the first layer deposition, the laser beam turns back immediately and continuously deposits the second layer. The maximum temperature in the melt pool of second layer deposition is 2193.5℃, which is 100℃ higher than that of the previous layer. As can be seen in fig. 6a the first layer is fully remelted, which leads to deeper remelting of the substrate and higher epitaxial grain growth in the [001] direction. The characteristic dimensions of the double layer deposit, i.e. the height, width and melting depth of substrate measured from simulation and experimental results are given in Table α. The large difference between simulation and experimental results is attributed to the intermittent deposition method used in the experiment. The deposition was stopped at the end of the first layer. The deposited track was naturally cooled for a few seconds while the laser beam moves back to the starting point for the second layer deposition. Therefore, due to the lower substrate preheat temperature, the melting depth of the substrate is much less in the experimental result.

Table 2. Comparison of the deposit dimensions of double layer clad between simulation and experimental results

	Deposit Track Height (mm)	Deposit Track Width (mm)	Substrate melting depth (mm)
Experimental (w/ cooling)	0.581	0.793	0.122
Simulation (w/o cooling)	0.404	0.672	0.205

Note: Deposition parameters: Laser power 200W, beam spot size 0.6 mm, scanning speed 5 mm/s, and powder flow rate 6 g/min

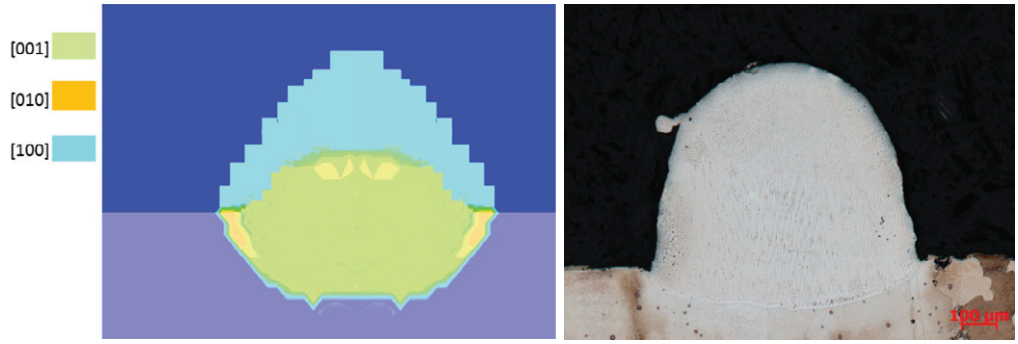

(a) (b)

Fig. 6. Cross-section geometry and grain orientation distributions of double layer deposition from simulation and experimental results respectively. Laser power 200W, beam spot size 0.6 mm, scanning speed 5 mm/s, and powder flow rate 6 g/min

5. Conclusion

In this study, a 3D numerical transient model for coaxial laser powder deposition process was developed to simulate the temperature field, fluid flow of melt pool, deposit geometry and crystalline growth orientation distribution.

The deposit height, width, and substrate melting depth agree well between experimental and simulation results. The modeling method can therefore be used to predict the deposit geometry with reasonable accuracy. The grain growth condition varies at different altitude of the melt pool, the [001] direction grains transform into equiaxial grains at certain height of the deposition layer. It can be seen that increasing linear energy makes the depth of the [001] direction grain decrease in the deposition track. Deposition with smaller laser power leads to a large [001] direction grain. The simulation results can predict this experimentally observed trend with reasonable error.

Acknowledgements

This work was supported by the NSFC (Grant No. 51175338). The authors would also like to thank Yanming Li, Henry Peng for their support in acquiring materials and assistance in obtaining the experimental results.

References

[1] Qi. H., Cai, G., Azer, M.: Application of laser powder deposition for turbine blade tip cap freeform fabrication. In: Proceedings of the 4th Pacific International Conference on Applications of Lasers and Optics (PICALO) (2010).

[2] Liu, Y., Li, Y., Cai, G., Peng, H., Qi, H., Erikson, C., Schoonover, J.: Laser Net Shape Manufacturing of Rene195. In: Proceedings of 27th International Congress on Applications of Lasers and Electro-Optics (ICALEO), (2008), Pages 777-781.

[3] Gaumann,M., Henry,S., Wagniere, J.-D., Kurz, W.: Expitaxial laser metal forming: analysis of microstrure formation. In: Materials Science and Engineering, (1999), A271, 232-241.

[4] Gaumann, M., Bezencon, C., Canalis, P. and Kurz, W.: Single-Crystal Laser Deposition of Superalloys: Processing - Microstructure Maps. In: Acta Materialia, (2001), 49, 1051-1062.

[5] Liu, W. and DuPont, J.N.: Effects of Melt-pool Geometry on Crystal Growth and Microstructure Development in Laser Surface-Melted Superalloy Single Crystals. Mathematical Modeling of Single Crystal Growth in a Melt Pool (Part I). In: Acta Mater (2004); 52: 4833-47.

[6] Liu, W. and DuPont, J.N.: Effects of Substrate Crystallographic Orientations on Crystal Growth and Microstructure Development in Laser Surface-melted Superalloy Single Crystals. Mathematical modeling of single-crystal growth in a melt pool (Part II). In: Acta Materialia. (2005) Vol. 53, no. 5, pp. 1545-1558.

[7] Park, J.-W., Babu, S.S.,Vitek, J.M., Kenik, E.A., David, S.A.: Stray Grain Formation in Single Crystal Ni-base Superalloy Welds. In: Journal of Applied Physics (2003) Volume:94,Number 6,4023-4029.

[8] Vitek, J.M.: The Effect of Welding Conditions on Stray Grain Formation in Single Crystal Welds-Theoretical Analysis. In: Acta Materialia, (2004), 53, 53-67.

[9] Anderson, T.D., DuPont, J.N. and DebRoy, T.: Origin of Stray Grain Formation in SX Superalloy Weld Pools from Heat Transfer and Fluid Flow Modeling, In: Acta Materialia, (2009) Volume: 58, Issue: 4, Pages: 1441-1454.

[10] Toyserkani, E., Khajepour, A. and Corbin. S.: Three-dimensional finite element modeling of laser cladding by powder injection: Effects of powder feedrate and travel speed on the process. In: Journal of Laser Applications (2003), 15(3):153–160.

[11] Qi, H., Mazumder, J., and Ki, H.: Numerical simulation of heat transfer and fluid flow in coaxial laser cladding process for direct metal deposition. In: Journal of Applied Physics (2006) 100, 024903, 2005.

[12] He,X., Mazumder, J.: Transport Phenomena During Direct Metal Deposition. In: Journal of Applied Physics (2007) 101, 053113.

[13] Peyre, P., Aubry, P., Fabbro, R., Neveu, R., Longuet, A.: Analytical and numerical modelling of the direct metal deposition laser process, In: Journal of Physics D: Applied Physics, (2008) 41 (2), art. no. 025403.

[14] Wen Shaoyi., Shin, Tung C.: Modeling of Transport Phenomena During the Coaxial Laser Direct Deposition Process. In: Journal of Applied Physics (2010) 108, 044908.

[15] He X., Yu G., Mazumder, J.: Temperature and Composition Profile During Double-track Laser Cladding of H13 Tool Steel. In: Journal of Applied Physics, D: Applied Physics (2010) 43, 015502.

[16] S.Mokadem, C.Bezencon, J.-M.Drezet, A.Jacot, J.-D.Wagniere, W.Kurz.: Microstructure Control During Single Crystal Laser Welding and Deposition of Ni-base Superalloys, In: Proceedings of Symposium on Solidification Processes and Microstructures TMS Annual Meeting, (2004).